Efficient Dynamic Focus Control for Three-Dimensional Imaging Using Two-Dimensional Arrays

Pai-Chi Li, *Senior Member, IEEE*, and Jing-Jung Huang

Abstract—**Dynamic receive focusing in ultrasonic array imaging involves extensive real-time computations and data communication. Particularly for three-dimensional imaging, using fully sampled, two-dimensional arrays, implementation of dynamic focusing can be extremely complicated because of the large channel count. In this paper, an efficient dynamic focus control scheme for a delay-and-sum-based beamformer is proposed. The scheme simplifies dynamic focus control by exploiting the range-dependent characteristics of the focusing delay. Specifically, the overall delay is divided into a range-independent steering term and a range-dependent focusing term. Because the focusing term is inversely proportional to range, approximation can be made to simplify dynamic focus control significantly at the price of minimal degradation in focusing quality at shallow depths. In addition, the aperture growth controlled by a constant $f_{/\text{number}}$ can also be utilized to devise a non-uniform quantization scheme for the focusing delay values. Efficacy of the proposed scheme is demonstrated using simulated beam plots of a fully sampled, two-dimensional array. Design procedures are also described in detail in this paper. One design example shows that, with the proposed dynamic focus control scheme, a 4096-element array only requires 227 independent controllers for the range-dependent focusing term. Moreover, only 28 non-uniform quantization levels are required to achieve the same focusing quality as that of a conventional scheme with 784 uniform quantization levels. The beam plots of a fully sampled array show that sidelobes are slightly increased below the −30 dB level for imaging depths less than 3 cm. At greater depths, there is no observable degradation.**

I. Introduction

DYNAMIC focusing provides high focusing quality over the entire depth of interest [1]–[11]. In an array imaging system, focusing is typically done by first delaying the backscattered signals based on the propagation path length difference. The delayed signals are then coherently summed across the array. This is also known as the delay-and-sum approach. Because medical ultrasound imaging primarily works in the near field region, the focusing delay for a particular channel changes as a function of range. Also, real-time interpolation is required to increase the effective data sampling rate for higher focusing accuracy. Considering the large number of system channels, implementation of dynamic focus control is complicated. The complexity becomes more significant when a fully sampled, two-dimensional array is used. In this case, the number of channels can be as large as several thousand. Thus, efficient dynamic focus control schemes must be developed to reduce the system complexity.

Imaging with two-dimensional arrays has gained broad interest in the past few years [12]–[19]. Potential advantages of such a system include reduced slice thickness, improved correction of sound velocity inhomogeneities, and real-time three-dimensional imaging. Despite the potential benefits, two-dimensional arrays have not been widely used in medical ultrasound. Particularly for three-dimensional imaging with two-dimensional (i.e., lateral and elevational) electronic steering, fully sampled arrays are required. The implementation is not possible with current electronic technologies unless major simplification can be achieved without significant image quality degradation.

In the field of digital beamformation using one-dimensional arrays, major research and development efforts have been spent on real-time interpolation and delay data generation [2]–[11]. Delay interpolation is required such that delay accuracy less than a sampling period can be achieved to improve focusing quality. Interpolation of the received RF signal can be implemented by using a finite impulse response (FIR) digital filter with the filter coefficients supplied by a delay control unit [3]. Alternatively, the RF signal can be demodulated to baseband to obtain a pair of quadrature-phased data [4], [5]. In this case, the fine time delay adjustment of the RF signal is implemented by rotating the phase of the complex baseband data. These methods are based on a uniformly sampling A-D converter (ADC). It was also shown that a variable sampling clock can be generated with sufficiently high accuracy for digital focusing without the need for a large amount of look-up memory and complex real-time delay computations [6]. Finally, an oversampled ADC using the delta-sigma modulator was proposed for digital beamformation that can significantly reduce the size, cost, and power consumption of the ultrasound beamformer [7]. Because it is possible to achieve a sampling frequency at least 32 times of the typical carrier frequency for diagnostic ultrasound, the delay accuracy is already sufficient, and interpolation is no longer required.

Another important area in digital beamformation is generation of the delay data. In [8], the delay profiles are generated on a dynamic and distributed basis with sparsely sampled reference delay data sets. The reference

Manuscript received June 1, 2001; accepted February 6, 2002.

The authors are with the Department of Electrical Engineering, National Taiwan University, Taipei, Taiwan, R.O.C. (e-mail: paichi@cc.ee.ntu.edu.tw).

0885-3010/$10.00 © 2002 IEEE

data sets are then expanded to the final delay values for each channel by a primary central delay controller and a secondary local delay controller. Dynamic delay data can also be generated using a simple state machine given the initial steering angle and the range clock [9]. Alternatively, a midpoint algorithm was also employed to generate delay values below a decimal point based on a focusing reference distance and integer focusing delay distances [10]. Another delay generator produces an exact solution of the delay equation within the quantization error of the delay unit for a given steering angle, focal depth, and transducer element [11]. The delay generator is also capable of steering the receive beam to a dynamically variable steering angle.

For three-dimensional imaging using two-dimensional arrays, major efforts have been spent in the areas of transducer technologies, performance analysis, and imaging techniques using sparse arrays [12]–[18]. However, beamformers specifically designed for reducing the complexity associated with fully sampled two-dimensional arrays have been lacking. It was mentioned in [7] that the delta-sigma-based beamformer may also be beneficial for two-dimensional arrays because of its reduced cost, size, and power consumption. Nonetheless, further simplification may still be required to reduce the complexity because of the large channel count of a fully sampled two-dimensional array. In [19], the system complexity is reduced by utilizing subarray processors. In this case, the steering component of the entire delay is implemented in the analog domain using a phase shift network. The phase-shifted analog signals for all of the channels within a subarray are summed together and sampled by an ADC. The focusing component of the entire delay is then applied to the sampled signal before the final beam sum is obtained. Although it is suggested that such a scheme can be implemented efficiently, a more systematic approach for determining the sub-array geometry for optimal focusing quality is still absent. Therefore, it is a primary purpose of this paper to provide such a systematic approach and to demonstrate its efficacy. Moreover, another purpose of this paper is to develop an approach for delay data approximation. With these, focusing quality of fully sampled two-dimensional arrays can be maintained while the system complexity can be greatly simplified.

The focus control scheme proposed in this paper breaks down the total delay into two terms. The first term is independent of range and is generally referred to as the beam steering term. The second term is inversely proportional to range and is referred to as the range focusing term. Note that the steering term only needs to be specified at the beginning of a beam, and, hence, it is relatively straightforward to implement. The range focusing term, on the other hand, needs to be dynamically updated and requires a complex focus control scheme. The proposed simplification scheme concentrates on the range focusing term, and the beam steering term is unaffected. It can be easily shown that any fixed error associated with the focusing term decreases as the range increases. Hence, approximation can be made by sacrificing focusing quality at shallow depths while maintaining the focusing quality at greater depths. The primary purpose of this paper is to describe details of the focus control scheme and to demonstrate its efficacy for three-dimensional imaging using two-dimensional arrays. By exploiting characteristics of the range-dependent focusing term, complexity is significantly reduced, and implementation of dynamic receive focusing becomes much more feasible. Performance of the proposed technique will be evaluated using simulated beam plots. A system architecture will also be described and compared with conventional architectures. Note that although the algorithms are developed for two-dimensional arrays, the same principles can be easily adopted to systems using one-dimensional arrays.

The paper is organized as follows. Focusing delays for both one-dimensional and two-dimensional arrays are derived in Section II. Design procedures of the proposed simplification scheme are described in Section III. In Section IV, simulations of focused beams at various angles and ranges are presented. The paper concludes in Section V with a comparison between the proposed approach and conventional approaches.

II. Fundamentals

For sector imaging using a one-dimensional array, the delay value of a particular channel can be represented as

$$t_{rx} = \left(\left((R\sin\theta - x)^2 + (R\cos\theta)^2 \right)^{1/2} - R \right) / c \approx -\frac{x\sin\theta}{c} + \frac{1}{R} \times \frac{x^2\cos^2\theta}{2c} \quad (1)$$

where x is the distance between the channel and the array center, c is the sound velocity, θ is the steering angle, and R is range of the focal point [9]. In (1), the Taylor's expansion is used, and the terms with an order higher than 2 are omitted for the approximation in the Fresnel region. Note that the first term in the approximation is independent of the range R and is also known as the beam steering term. The second term is known as the range focusing term and is proportional to $1/R$. For fixed focusing at (R, θ), the delays remain constant at all ranges along the same beam line. In this case, delays can be pre-computed and loaded into the beamformer at the beginning of each beam. For dynamic focusing, on the other hand, the system focuses at every range along the beam. Therefore, the range focusing term needs to be constantly updated. The beam steering term, on the other hand, is a fixed value, given the steering angle, and does not need to be dynamically updated.

Delay updates can be done by either utilizing a central controller to compute the delays and communicate with each channel or by having each channel autonomously determine the delay values based on some initial parameters set up at the beginning of each beam. In either case, a parameter Φ can be defined as

$$\Phi = x^2\cos^2\theta. \quad (2)$$

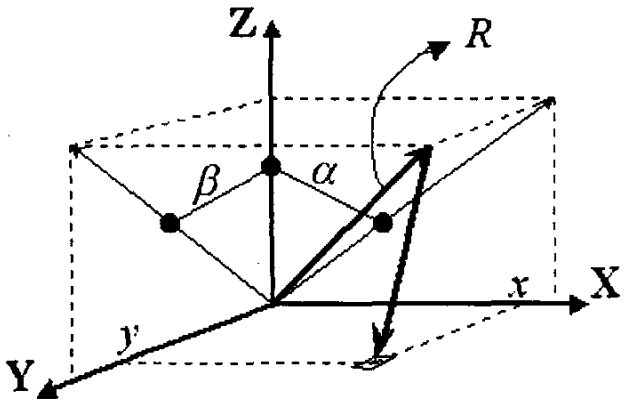

Fig. 1. Coordinates of the three-dimensional imaging space. The array is in the x-y plane, z is the depth direction, and α and β are the lateral and elevational steering angles, respectively.

By specifying the beam steering term (i.e., $-x \sin\theta/c$) and Φ at the beginning of an ultrasound beam, the overall delay t_{rx} can be found at every range R. Because the focusing term is an even function of x with the Fresnel approximation (i.e., Φ at x is the same as Φ at $-x$), the number of delay controllers for the range-dependent term can be reduced by 50% because of the symmetry.

For three-dimensional imaging using a two-dimensional array, the delay can be derived in a similar fashion. As shown in Appendix A, approximation of the total delay in this case becomes

$$t_{rx} \approx -\frac{(x\tan\alpha + y\tan\beta)}{c(1+\tan^2\alpha+\tan^2\beta)^{1/2}} + \frac{1}{R} \times \frac{(x^2+y^2)+(x\tan\beta - y\tan\alpha)^2}{2c(1+\tan^2\alpha+\tan^2\beta)} \quad (3)$$

where (x, y) represents a channel in the two-dimensional array with the array center being the origin; α and β are the steering angles along the lateral direction and the elevational direction, respectively. Again, the first term only depends on steering angles and is referred to as the beam steering term. The second term is inversely proportional to range and is referred to as the range focusing term. Coordinates used in (3) are also shown in Fig. 1. In this case, the parameter Φ for a two-dimensional array can be defined as

$$\Phi = \frac{(x^2+y^2)+(x\tan\beta - y\tan\alpha)^2}{1+\tan^2\alpha+\tan^2\beta}. \quad (4)$$

Note that the symmetry for the second term is still valid because the Φ value of the channel at (x, y) is identical to that of the channel at $(-x, -y)$. Therefore, for an N-by-N two-dimensional array, the number of delay controllers for the range-dependent term can be reduced to $N^2/2$. Apparently, further simplification is required for two-dimensional arrays even if the symmetric property is used.

Fig. 2 shows the block diagram of a dynamic focus control scheme. In this case, the steering term and Φ are sent to the delay controller for channels at (x, y) and $(-x, -y)$

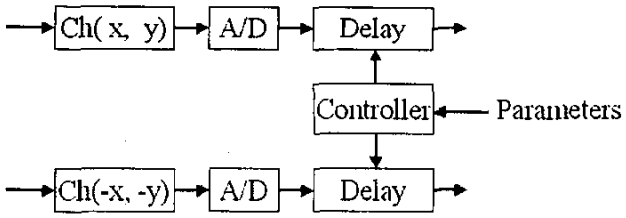

Fig. 2. A block diagram of the beamformer.

at the beginning of each beam. Based on the two parameters, the controller then calculates the overall delay at each range. Such a delay control scheme is very general and can be extended to a broad range of beamformer architectures. For example, if real-time baseband interpolation is used, the overall delay can be further converted into a course time delay and a fine phase delay without changing the basic structure of the proposed scheme. Based on the basic control structure shown in Fig. 2, the goal of the proposed method is to simplify the delay controller by approximating the term Φ. The steering term is unaffected in the proposed method.

Another important feature of dynamic focusing in array imaging is the use of a constant $f_{/\text{number}}$ to control aperture growth as the range increases. At small ranges, only channels close to the beam origin are used. As the range increases, more channels become active until the array is fully open. Therefore, the Φ value related to the outside channels (i.e., large (x, y)'s) may tolerate bigger errors as they are associated with a larger R. As will be shown later, this characteristic is also critical in developing the dynamic focus control scheme described in the next section.

III. The Dynamic Focus Control Scheme

There are three main components of the proposed dynamic focus control scheme.

A. Grouping of Adjacent Channels

The first component is grouping of adjacent channels. In other words, the array is divided into segments (i.e., sub-arrays), and the same Φ value is used by all of the channels in the same segment. Thus, the true value of Φ is approximated by another value Φ' and

$$\Phi' = \Phi + \delta \quad (5)$$

where δ is the approximation error. Consequently, the total delay becomes

$$t'_{rx} = t_{rx} + \frac{\delta}{2Rc} \quad (6)$$

where t_{rx} is the original delay and t'_{rx} is the approximated delay. The second term in (6) is viewed as a range focusing error, which may cause image quality degradation. Fig. 3

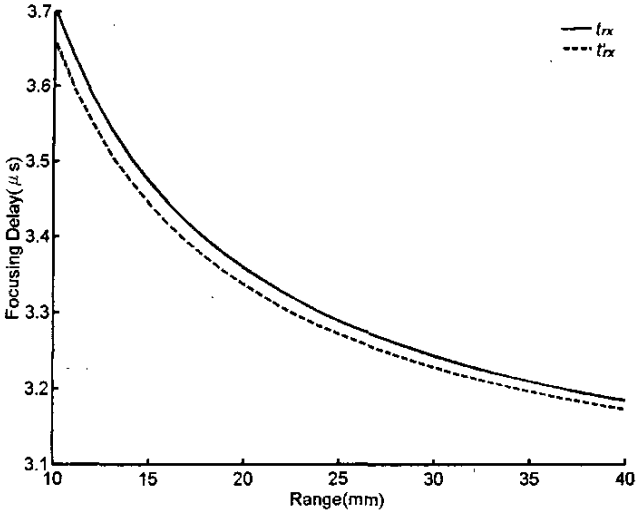

Fig. 3. Quantization error of the range focusing term decreases as a function of range.

shows a typical example of t'_{rx} and t_{rx}, where the delay error δ corresponds to one of the typical imaging conditions, and the delay curves are shown for the range from 10 to 40 mm. As expected, the delay error decreases as the range R increases. Consequently, the image quality degradation occurs only at smaller ranges, and the error is negligible when the range is sufficiently large.

Determination of the sub-array geometry is critical in minimizing the focusing error. The proposed scheme develops the geometry at zero steering angles (i.e., $\alpha = \beta = 0°$) and then applies the result to all beams. According to (4), $\Phi = x^2 + y^2$ when $\alpha = \beta = 0°$. Thus, a constant Φ corresponds to a circle on the aperture with the array center being the origin. It becomes obvious to divide the array into concentric rings, and channels on the same ring can share the same Φ. To reduce potential approximation errors for off-center beams, each ring is further divided into smaller segments. Following this approach and derivation outlined in Appendix B, the length Δn of a particular ring along the radial direction is determined by

$$\Delta n \leq \sqrt{(n-0.5)^2 + 16(n-0.5)\varepsilon_1 G \times f_{/\text{number}}} - (n-0.5) \quad (7)$$

where n is the inner radius of the ring, ε_1 is a predetermined maximum delay error normalized to the wavelength, and G is a correction factor defined as

$$G = \exp\left[\gamma\left(\frac{n}{n_0} - 1\right)\right] \quad (8)$$

where n_0 is the radius of the first (smallest) ring and γ is an adjustable parameter. In general, G can be any monotonically increasing function of n/n_0. The purpose of G is to increase the length of outer rings further, as they are active only at larger ranges. Note that both n and Δn are defined in terms of number of array elements assuming half-wavelength pitch is used.

In addition to the correction factor G, each ring is also partitioned into smaller segments to further reduce the errors at off-center beams. The radial length of each segment is determined based on (7). The angle ξ of each segment, on the other hand, can be determined by

$$\xi = \frac{M \times \Delta n}{n} \quad (9)$$

where M is a pre-specified aspect ratio. Through this procedure, array partition can be implemented. Channels inside the same segment use the same Φ' value and, thus, share the same delay controller. Φ' can be defined as the mean of all Φ values within the same segment. The various parameters used in this discussion are graphically defined in Fig. 4(a), and a typical segmentation pattern is shown in Fig. 4(b). Let $\varepsilon_1 = 0.05$ (i.e., the maximum delay error is 1/20 of the wavelength), $n_0 = 4$, $\gamma = 0.15$, $M = 3$, and $f_{/\text{number}} = 2$, the 64-by-64 array (totally 4096 channels) can be controlled by using only 227 controllers. Note that the total number of segments is 454, and the 50% reduction is due to the even symmetry of Φ. These parameters will be used in subsequent simulations.

B. Quantization of Φ

For an N-channel array with a half wavelength pitch and ±45° maximum steering angles in azimuth, the number of beams is $\sqrt{2}N$, assuming Nyquist beam spacing (i.e., $\sqrt{2}N = (\sin(45°) - \sin(-45°))/bs$, where bs is the Nyquist beam spacing defined as bs = (wavelength/2 · aperture_size) = $1/N$). For an N-by-N array with ±45° maximum steering angles in both α and β, the number of beams becomes $2N^2$. Consequently, Φ needs to be specified for $2N^4$ (i.e., N^2 channels times $2N^2$ beams) different combinations. The purpose here is to develop a quantization scheme for Φ such that optimal focusing performance is maintained while minimizing the total number of quantization levels. Note that such a scheme can reduce the memory requirement of the controller. However, the overall control bandwidth is still not affected.

One example is shown in Fig. 5(a), where the horizontal axis shows extent of Φ, and the vertical axis is the range. Because of the $f_{/\text{number}}$ aperture growth control, extent of Φ changes with range, as the outside channels do not become active until a larger range is reached. Thus, a smaller quantization step is required when Φ is small, and larger quantization errors may be accepted when Φ is large. In other words, non-uniform quantization of Φ can be implemented.

Following the details described in Appendix C, the number of quantization levels L can be obtained as

$$L = \frac{N}{8\sqrt{2} \times \varepsilon_2 \times f_{/\text{number}}} \quad (10)$$

where ε_2 defines the maximum quantization error, and the

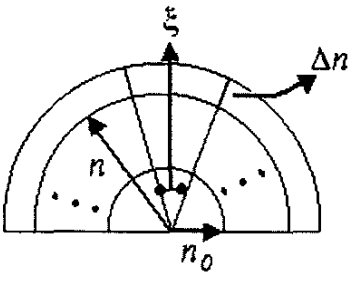

FIG. 4(a)

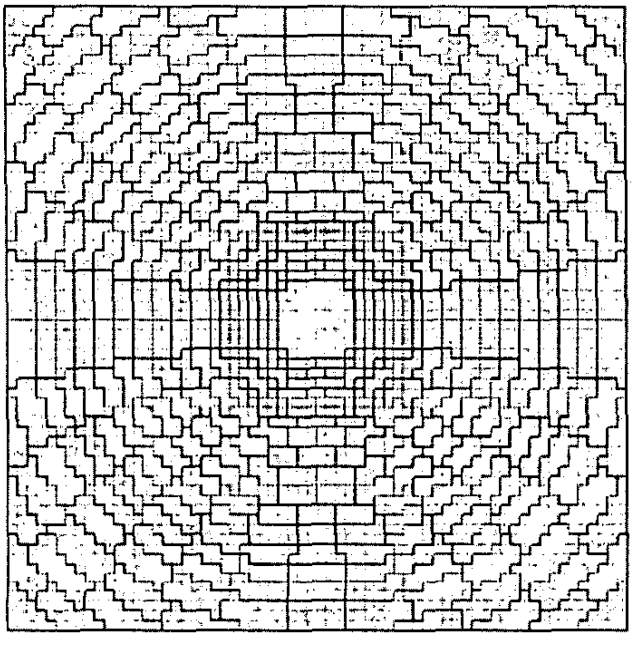

FIG. 4(b)

Fig. 4. a) Definition of parameters; b) a segmentation pattern of a two-dimensional array.

quantized value of Φ at level i is

$$\Phi_i = 8 \times \left(\varepsilon_2 \times \lambda \times f_{/\text{number}}\right)^2 \times \left(2i^2 - 2i + 1\right), i \in [1, L] \quad (11)$$

where λ is the wavelength at the carrier frequency. If a uniform quantizer is used in the same situation, approximately L^2 levels need to be used to obtain the same level of accuracy.

An example of the non-uniform quantization is shown in Fig. 5(b). Let $N = 64$, $\varepsilon_2 = 0.1$, carrier frequency = 4 MHz, and $f_{/\text{number}} = 2$, there are only 28 quantization levels. Among these, the 28th quantization level is never used if the grouping scheme shown in Fig. 4(b) is used. Therefore, only 27 levels are required in this case.

C. Range Offset

Given a Φ', a fixed error is present at all ranges. The error can be redistributed by adding a fixed correction term.

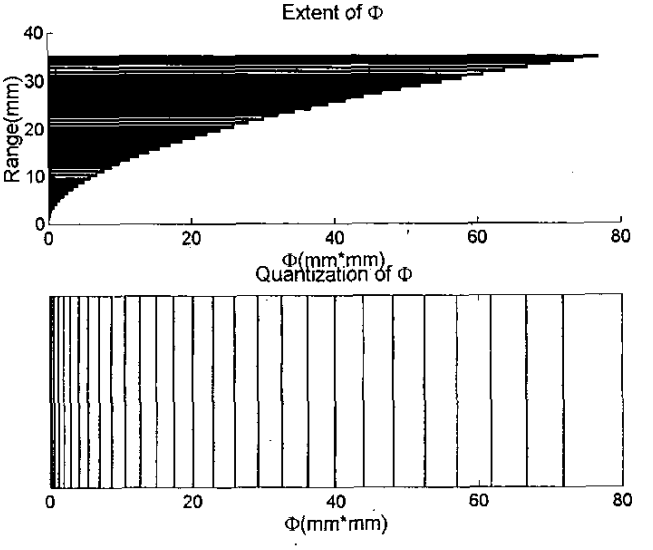

Fig. 5. a) Extent of Φ (horizontal) as a function of R (vertical); b) non-uniform quantization of Φ. At larger Φ's, coarser quantization steps can be used.

Define t''_{rx} as the following

$$\begin{aligned} t''_{rx}(R) &= t'_{rx}(R) - \frac{\delta}{2R_0c} \\ &= t_{rx}(R) + \frac{\delta}{2Rc} - \frac{\delta}{2R_0c} \end{aligned} \quad (12)$$

where R_0 is the depth with no focusing error. Compared with the uncompensated approximation, the focusing error becomes q times the original error at range R, where q is defined as

$$q(R) \equiv \left| \left(\frac{\delta}{2Rc} - \frac{\delta}{2R_0c}\right) \Big/ \frac{\delta}{2Rc} \right| = \frac{|R_0 - R|}{R_0}. \quad (13)$$

By properly selecting R_0, q can be less than 1 at all ranges. The effect of range offset on the range-dependent focusing term is illustrated in Fig. 6 with $R_0 = 60$ mm.

IV. Simulation Results

Simulations based on the angular spectrum method were performed to investigate the efficacy of the proposed approach. The angular spectrum method simulates wave propagation in the spatial frequency domain [20]. First, the initial sound field is transformed to the spatial frequency domain via two-dimensional Fourier transform. Wave propagation is simulated by multiplying spatial spectrum of the sound field with the following transfer function

$$H(f_x, f_y, \Delta z) = e^{jk\Delta z\sqrt{1-\lambda^2\left(f_x^2+f_y^2\right)}} \quad (14)$$

where f_x and f_y are the spatial frequencies corresponding to x and y, respectively; Δz is the propagation distance; and k is the wave number. After propagation, two-

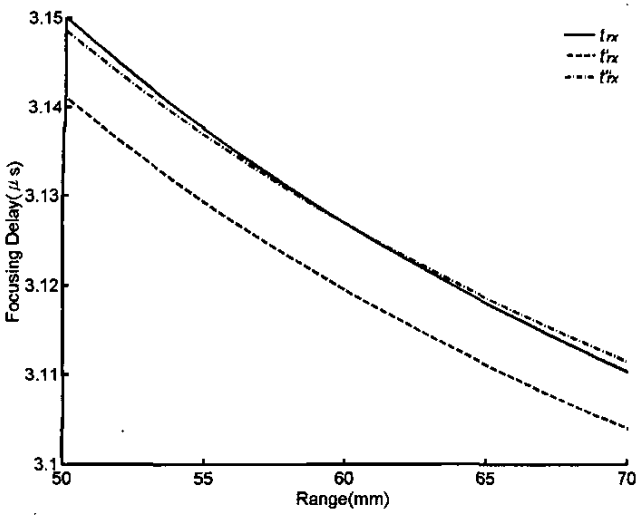

Fig. 6. The offset compensation technique; 60 mm is the range with no focusing error.

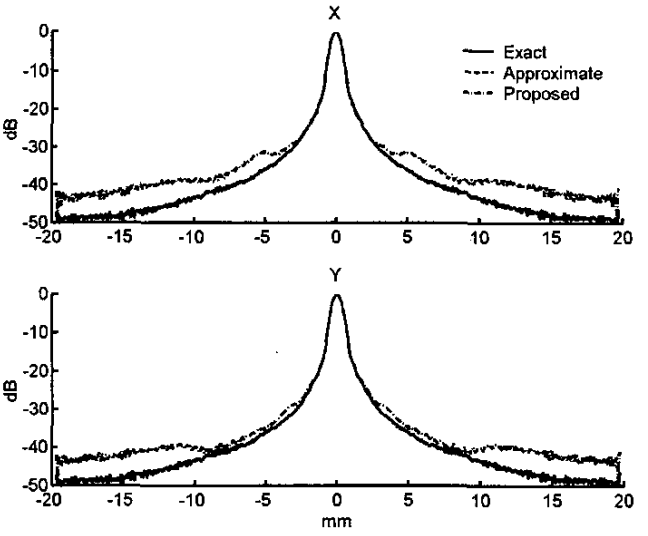

Fig. 7. Simulation results at 4 MHz. $\alpha = 0°$, $\beta = 0°$, $R = 15$ mm. Projections of the three methods in x (upper) and y (lower).

dimensional inverse Fourier transform is then taken to obtain the sound field at the new depth. Such a process can be repeated over all frequency components for pulse wave propagation. The pulse wave sound field can be obtained by summing results at all frequencies of interest.

Simulated beam patterns at several steering angles and ranges are demonstrated from Fig. 7 to 10. Only one-way receive beam patterns are shown. The corresponding two-way response can be obtained by multiplying the fixed focus transmit beam with the dynamic focus receive beam. A 4-MHz, 64-by-64 two-dimensional array was assumed. Each figure shows the projection of the beam plots along the x (upper) and the y (lower) directions. In each figure, the solid line represents beamforming results using ideal delay values (i.e., no Fresnel approximation). The dashed line shows the results based on the approximated delay values described in (6). The results of the proposed method are shown by the dot-dashed line. A depth of 60 mm was used to offset the focusing error (i.e., $R_0 = 60$ mm).

Fig. 7 demonstrates the beam plots for $\alpha = 0°$, $\beta = 0°$, and $R = 15$ mm. It is shown that at 15 mm, sidelobes are slightly elevated from the ideal case because of delay approximation. Nonetheless, the sidelobes are mainly under the -30 dB level, and the mainlobe width is unchanged. Such errors decreased as the range increased to 30 mm. The three beam patterns for $\alpha = 0°$, $\beta = 0°$, $R = 30$ mm are shown in Fig. 8. In this case, the three beam patterns are almost identical. Simulated sound fields at nonzero steering angles are demonstrated in Figs. 9 and 10. Fig. 9 shows the beam patterns for $\alpha = 20°$, $\beta = 40°$, $R = 15$ mm, and Fig. 10 shows the beam patterns for $\alpha = 20°$, $\beta = 40°$, $R = 30$ mm. In this case, slight steering errors are present.

Mean and standard deviation of delay errors as a function of steering angles are shown in Fig. 11 ($R = 15$ mm) and Fig. 12 ($R = 45$ mm), respectively. The delay errors are normalized to the wavelength at the center frequency. At each range, the statistics are calculated from all channels given an (α, β) combination. In each panel, the horizontal axis indicates $\sin(\alpha)$, and the vertical axis indicates $\sin(\beta)$. The mean values are shown in Fig. 11(a), and the standard deviation values are shown in Fig. 11(b). In each figure, the four images are for the Fresnel approximation (upper left), grouping of adjacent channels (upper right), non-uniform quantization (lower left), and the combination of both approaches (lower right). The results for $R = 45$ mm are shown in Fig. 12. As expected, both the mean and standard deviation of the focusing errors decrease when the range moves from 15 to 45 mm. At 60 mm, the errors are at the smallest because of the range offset. The mean and standard deviation then gradually increase after 60 mm. Note that at 15 mm, the aperture

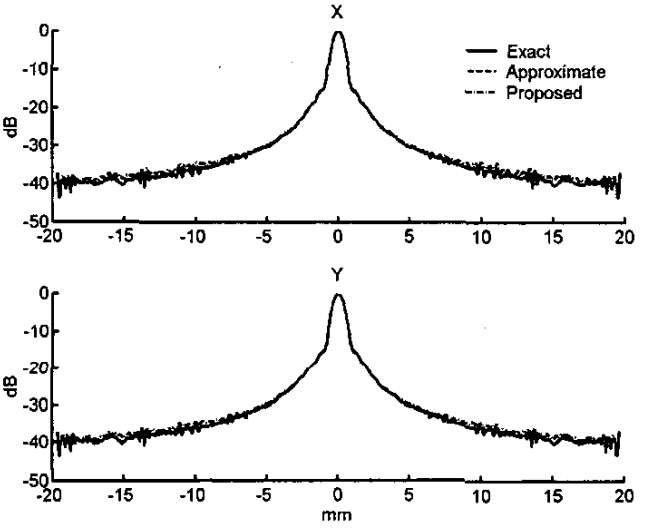

Fig. 8. Simulation results at 4 MHz. $\alpha = 0°$, $\beta = 0°$, $R = 30$ mm. The format is the same as that in Fig. 7.

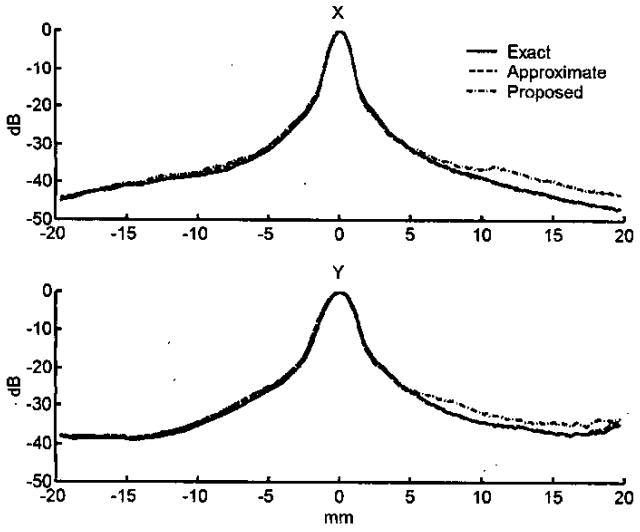

Fig. 9. Simulation results at 4 MHz. $\alpha = 20°$, $\beta = 40°$, $R = 15$ mm. The format is the same as that in Fig. 7.

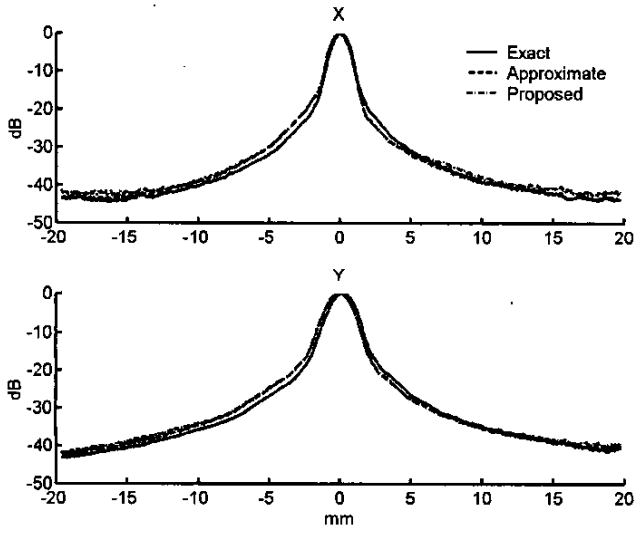

Fig. 10. Simulation results at 4 MHz. $\alpha = 20°$, $\beta = 40°$, $R = 30$ mm. The format is the same as that in Fig. 7.

is not fully open, thus making the errors resulting from Fresnel approximation relatively small. Also note that a mean error of 0.02 wavelength is equivalent to uniform delay quantization with a step size of 0.04 wavelength (i.e., mean phase error is $2\pi/25$). The errors can be reduced by employing smaller quantization steps.

V. Discussion and Concluding Remarks

The proposed control scheme only requires two parameters (i.e., the steering term and Φ) at the beginning of each beam. The $1/R$ term can be implemented by using a single bit control signal. Such a control signal is generally 0 unless an additional delay is required. The memory requirement of such a single-bit control scheme is around 34 Kbits assuming 128-MHz delay resolution and a 20-cm imaging depth. Thus, the 27 single-bit control signals used in the simulations can be stored in less than a 1-Mbit memory (27×34 Kbits). Note that the 128-MHz clock rate is used as an example. In practice, the delay update rate does not need to be as high as the sampling frequency. In this case, the complexity can be further reduced. Fig. 13 shows a possible architecture to take advantage of the given control scheme, where focusing patterns are stored in the control signal table, and multiplexers are used to replace complex delay controllers. It must be noted that the reduced memory requirement caused by non-uniform quantization does not reduce the overall control bandwidth. In addition, the scheme shown in Fig. 13 may be implemented as a centralized controller (i.e., a single multiplexer) or a distributed controller (i.e., multiple multiplexers), depending on the control bandwidth requirement of the imaging system.

Comparisons of the conventional architecture and the proposed architecture are listed in Table I. For a 64-by-64 two-dimensional array, there are 4096 channels. The conventional architecture may exploit the delay symmetry and uses 2048 controllers. In addition, each delay controller may or may not require a complex algorithm to compute the delay changes in real time. Through grouping of adjacent channels, the number of controllers is reduced to 227. Also, each controller requires only a small table and a multiplexer. The size of the multiplexer can be further reduced. As shown in Fig. 14, not all of the connections between selection signals and delay control signals are needed. As shown in Fig. 14, only 20% of the total possible connections are required. Thus, further reduction of the multiplexer size is possible. Because of the significant reduction in the number of focus controllers and the number of quantization steps, the multiplexer architecture in combination with the single-bit control scheme becomes a realistic and effective focus control scheme. Again, such a scheme may be used as a centralized controller or a distributed controller, depending on the control bandwidth requirement.

The method simplifies control of the focusing delay, but the steering term in (3) is still needed. For 4096 channels and 8192 beams, there are totally 32 M words of initial delays. The word length in this case is determined by the extent of the steering term and the desired focusing accuracy. The 227 segments for the range focusing term require a memory space of 1.8 M words. Because the two parameters are only needed at the beginning of a beam, and dynamic range update is not required, data communication requirements are manageable with current technologies. Alternatively, the approach proposed in [19] for the steering component can be used.

The methods can also be applied to one-dimensional arrays. Because the total number of channels for a one-dimensional array is not as large, grouping of the adjacent channels may not be necessary. Nonetheless, non-uniform quantization can still be employed. To avoid image quality degradation in the near field, more quantization levels can be used. In other words, the delay error can be easily

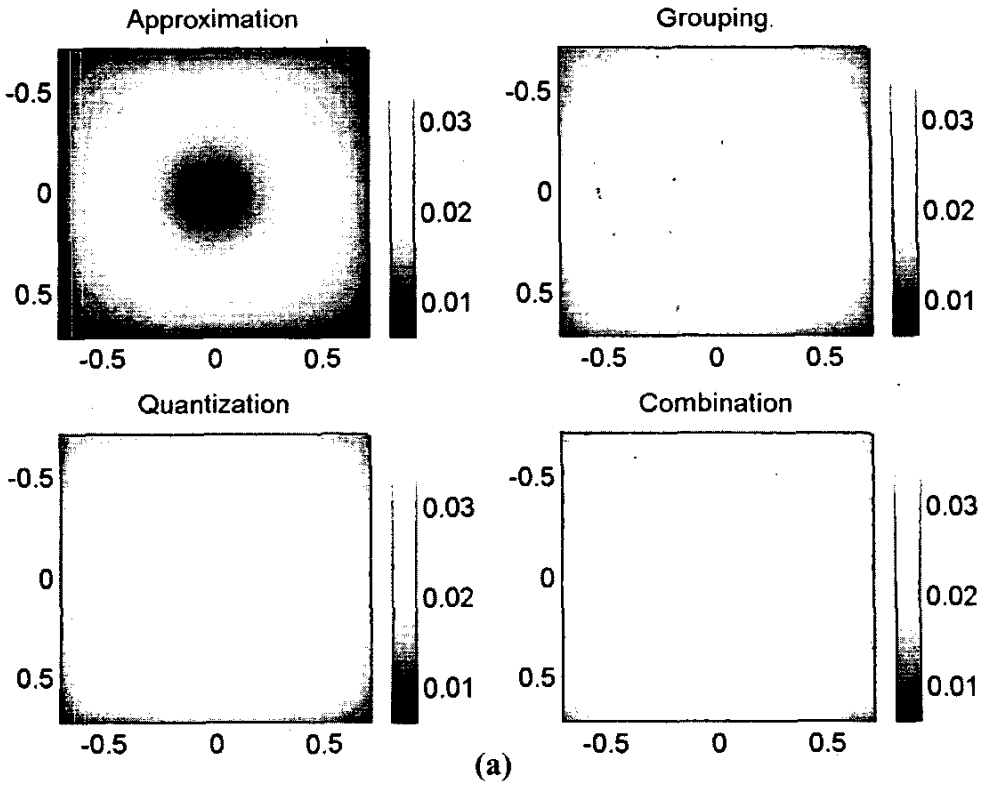

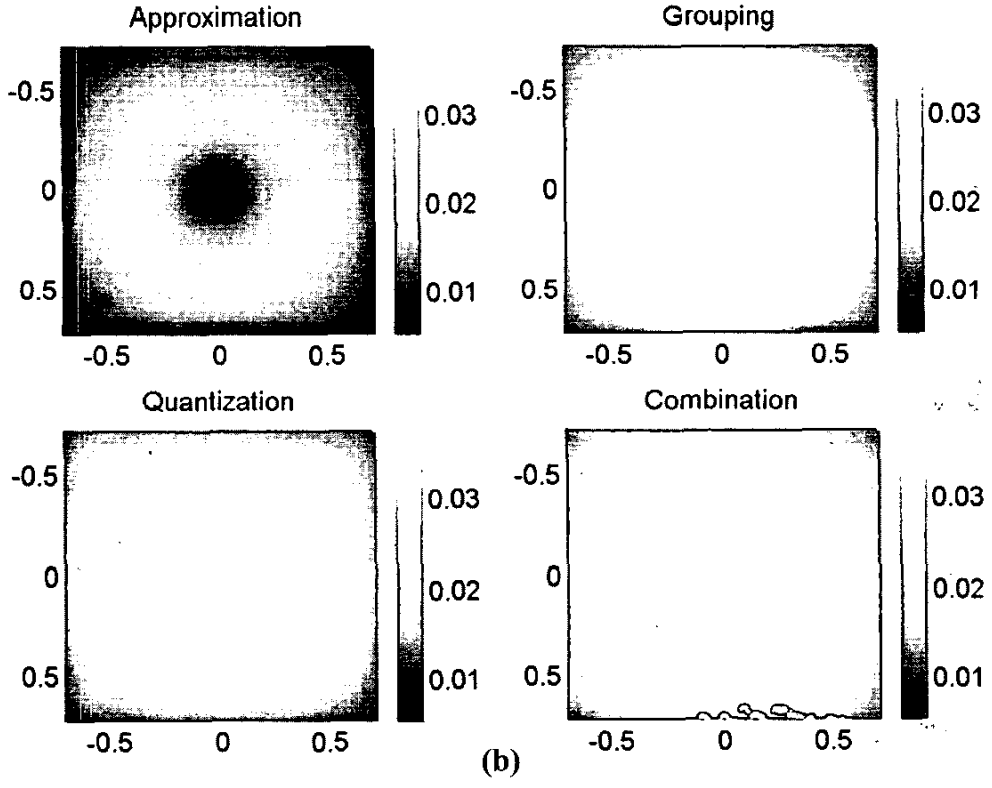

Fig. 11. Mean (a) and standard deviation (b) of focusing errors as a function of steering angles at 15 mm. Results from the Fresnel approximation (upper left), grouping of adjacent channels (upper right), non-uniform quantization (lower left), and combination of both approaches (lower right) are shown.

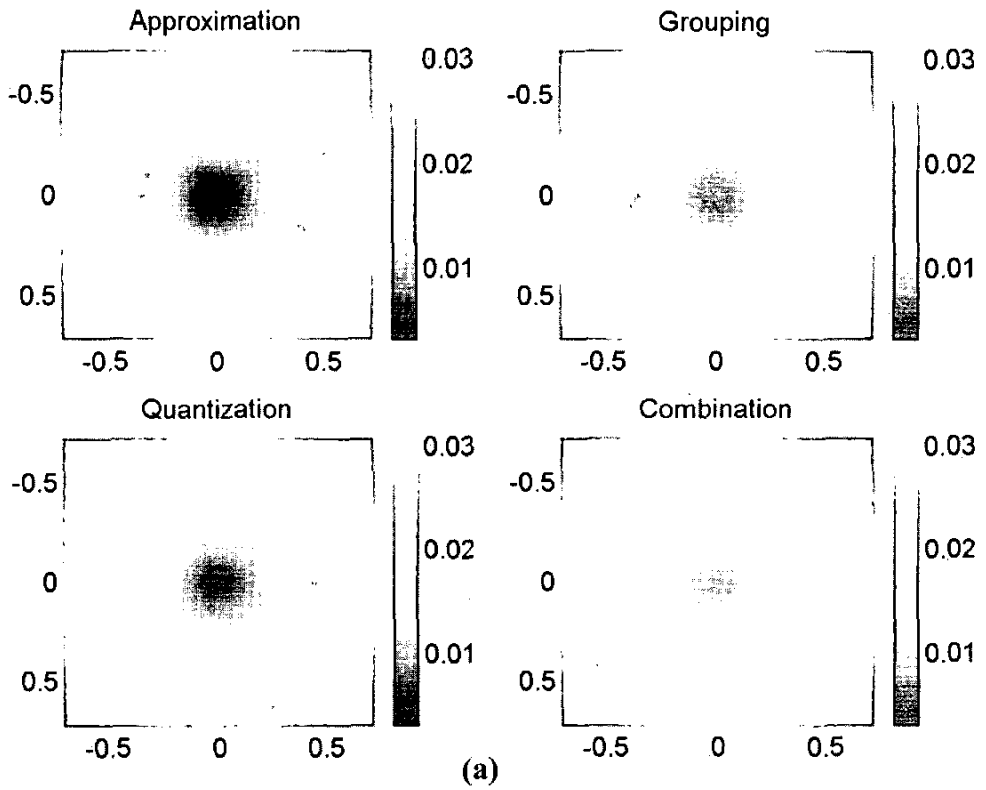

Fig. 12. Mean (a) and standard deviation (b) of focusing errors as a function of steering angles at 45 mm. Results from the Fresnel approximation (upper left), grouping of adjacent channels (upper right), non-uniform quantization (lower left), and combination of both approaches (lower right) are shown.

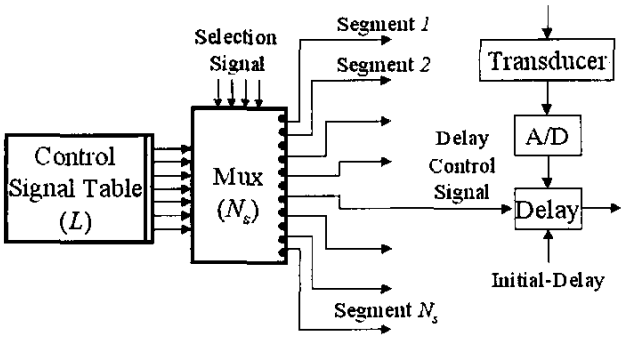

Fig. 13. A possible implementation of the proposed delay control scheme.

TABLE I
COMPARISON OF DIFFERENT APPROACHES.

	Original	Proposed
Number of controllers	2048	227
Image quality	Excellent	Slight degradation at shallow depths
Steering table	32 M words	32 M words
Φ Table	16 M words	1.8 M words
Control signal table	None	<1 Mb

reduced to be less than that generated by a sampler working at 32 times of the carrier frequency. In this case, the overall architecture is still simpler than the conventional approaches.

APPENDIX A

Define the plane $z = 0$ as the aperture plane. Assume that the distance between the channel (x, y) (i.e., with three-dimensional Cartesian coordinate $(x, y, 0)$) and the focal point (fp_x, fp_y, fp_z) is D, and the distance between the array center (i.e., $(0, 0, 0)$) and the focal point is R; the following equations can be derived based on the notations defined in Fig. 1.

$$\begin{cases} D^2 = (fp_x - x)^2 + (fp_y - y)^2 + fp_z^2 \\ R^2 = fp_x^2 + fp_y^2 + fp_z^2 \\ fp_x = fp_z \times \tan\alpha \\ fp_y = fp_z \times \tan\beta \end{cases} \tag{A1}$$

$$R^2 = fp_z^2 \times (1 + \tan^2\alpha + \tan^2\beta). \tag{A2}$$

Define P as

$$P \equiv \sqrt{1 + \tan^2\alpha + \tan^2\beta}, \tag{A3}$$

then fp_z can be rewritten as

$$fp_z = \frac{R}{P} \tag{A4}$$

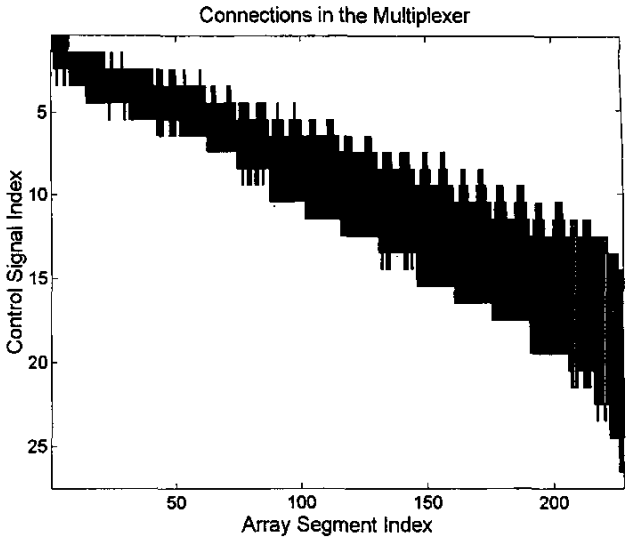

Fig. 14. Connections in the multiplexer. The array segment index is arranged from the array center to outer segments. It is shown that not all possible connections are needed.

and

$$\begin{aligned} D^2 &= \left(fp_x^2 - 2fp_x x + x^2\right) + \left(fp_y^2 - 2fp_y y + y^2\right) + fp_z^2 \\ &= R^2 + x^2 + y^2 - \frac{2R}{P}\left(x\tan\alpha + y\tan\beta\right). \end{aligned} \tag{A5}$$

If R satisfies the following condition

$$R^2 \gg \left(x^2 + y^2\right). \tag{A6}$$

then the distance D can be represented as

$$\begin{aligned} D &= R\left[1 + \frac{(x^2+y^2)}{R^2} - \frac{2}{RP}\left(x\tan\alpha + y\tan\beta\right)\right]^{1/2} \\ &\approx R\left[1 + \frac{(x^2+y^2)}{2R^2} - \frac{1}{RP}\left(x\tan\alpha + y\tan\beta\right)\right. \\ &\quad \left. - \frac{1}{8} \times \frac{4}{R^2P^2}\left(x^2\tan^2\alpha + y^2\tan^2\beta + 2xy\tan\alpha\tan\beta\right)\right] \\ &= R - \frac{x\tan\alpha + y\tan\beta}{P} + \frac{(x^2+y^2) + (x\tan\beta - y\tan\alpha)^2}{2RP^2}. \end{aligned} \tag{A7}$$

The receive delay of channel (x, y) relative to array center is

$$\begin{aligned} t_{rx} &= \frac{D - R}{c} \\ &= -\frac{x\tan\alpha + y\tan\beta}{c\sqrt{1 + \tan^2\alpha + \tan^2\beta}} \\ &\quad + \frac{(x^2+y^2) + (x\tan\beta - y\tan\alpha)^2}{2Rc(1 + \tan^2\alpha + \tan^2\beta)}. \end{aligned} \tag{A8}$$

Thus, the range dependent focusing parameter Φ can be defined as

$$\Phi = \frac{(x^2+y^2) + (x\tan\beta - y\tan\alpha)^2}{(1 + \tan^2\alpha + \tan^2\beta)}. \tag{A9}$$

APPENDIX B

Letting r represent the distance between channel (x, y) and the array center (i.e., $r^2 = x^2 + y^2$), we have the following equation for the center beam (i.e., $\alpha = \beta = 0°$):

$$\Phi(r)\Big|_{\alpha=\beta=0°} = r^2. \tag{B1}$$

The parameter r can also be viewed as the radius of a ring on the aperture with the array center being the origin. Grouping of adjacent channels is done by dividing the aperture into several concentric rings, and then each ring is further partitioned into smaller segments.

The radius r of each ring is determined based on uniform sampling of the term $\Phi/2Rc$. Hence, the difference δ_S between the Φ values at $r + \Delta r$ and at r becomes

$$\begin{aligned}\delta_S &= [\Phi(r + \Delta r) - \Phi(r)]\Big|_{\alpha=\beta=0°} \\ &= (r + \Delta r)^2 - r^2 \\ &= 2r(\Delta r) - (\Delta r)^2.\end{aligned} \tag{B2}$$

Let ε_1 be the desired maximum quantization error normalized to the wavelength λ, the following inequality can be obtained:

$$\frac{\delta_S}{2R} \le 2\varepsilon_1 \lambda G \tag{B3}$$

where the factor of 2 converts the maximum focusing error to an equivalent quantization interval. G is a correction term that will be defined later. Since $f_{/\text{number}} = R/2r$, we have

$$\delta_S \le 8r\varepsilon_1 \lambda G \times f_{/\text{number}}. \tag{B4}$$

After some arrangements, the following equations can be obtained

$$(\Delta r)^2 + 2r(\Delta r) - 8r\varepsilon_1 \lambda G \times f_{/\text{number}} \le 0 \tag{B5}$$

and

$$\Delta r \le \sqrt{r^2 + 8r\varepsilon_1 \lambda G \times f_{/\text{number}}} - r. \tag{B6}$$

Given the pitch of the array, (B6) can also be represented in terms of the number of channels. For one-half wavelength, fully sampled arrays, we have

$$r = (n - 0.5) \times \text{pitch} \tag{B7}$$

and

$$\Delta r = \Delta n \times \text{pitch}. \tag{B8}$$

Hence, the radial length of each ring in terms of the number of channels becomes

$$\Delta n \le \sqrt{(n - 0.5)^2 + 16(n - 0.5)\varepsilon_1 G \times f_{/\text{number}}} - (n - 0.5). \tag{B9}$$

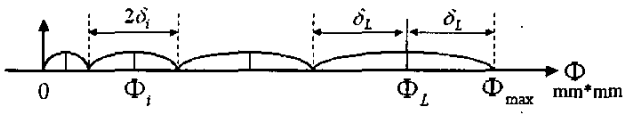

Fig. 15. Non-uniform quantization of Φ.

The function G is used to increase the length of outer rings further, as they are active only at larger ranges. It can be any function that monotonically increases with n/n_0. In this paper, it is defined as

$$G = \exp\left[\gamma\left(\frac{n}{n_0} - 1\right)\right] \tag{B10}$$

where γ is an adjustable parameter, and n_0 is the radius of the smallest ring.

Finally, each ring is further partitioned into smaller segments. The angular span of each segment can be defined as

$$\xi = \frac{M \times \Delta n}{n} \tag{B11}$$

where M is an aspect ratio of the segment. Definitions of the parameters used in this appendix are also illustrated in Fig. 4(a).

APPENDIX C

At zero steering angles, the maximum value of Φ is

$$\Phi_{\max} = r_{\max}^2 \tag{C1}$$

where $r_{\max}$ is the largest radius on the array. For an N-by-N array,

$$r_{\max} = \frac{N}{\sqrt{2}} \times \text{pitch}. \tag{C2}$$

The purpose of non-uniform quantization is to determine the number of quantization levels L and the quantization interval for each level between 0 and $\Phi_{\max}$ given a pre-specified maximum quantization error. The design strategy can be illustrated using the one-dimensional plot shown in Fig. 15. Let the quantization interval at a radius r be $2\delta(r)$, we have

$$\frac{\delta(r)}{2R} = \varepsilon_2 \lambda \tag{C3}$$

where λ is the wavelength at the carrier frequency, and ε_2 is the pre-specified maximum focusing error normalized to the wavelength. Because $f_{/\text{number}} = R/2r$, we have

$$\delta(r) = 4\varepsilon_2 \lambda r \times f_{/\text{number}}. \tag{C4}$$

If r is divided into L levels as the following

$$r_i = \frac{(2i - 1)}{2L} r_{\max} \quad i \in [1, L], \tag{C5}$$

then

$$\Phi_{\max} = \sum_{i=1}^{L} 2\delta(r_i). \tag{C6}$$

Thus

$$\begin{aligned} r_{\max}^2 &= 8\varepsilon_2\lambda \times f_{/\text{number}} \times \sum_{i=1}^{L} r_i \\ &= 8\varepsilon_2\lambda \times f_{/\text{number}} \times \frac{L(r_1 + r_L)}{2} \\ &= 4\varepsilon_2\lambda L \times f_{/\text{number}} \times r_{\max}. \end{aligned} \tag{C7}$$

The number of levels becomes

$$\begin{aligned} L &= \frac{r_{\max}}{4\varepsilon_2\lambda \times f_{/\text{number}}} \\ &= \frac{N}{8\sqrt{2} \times \varepsilon_2 \times f_{/\text{number}}}. \end{aligned} \tag{C8}$$

Each entry in the Φ table can then be expressed as

$$\Phi_1 = \sum_{l=1}^{i-1} 2\delta_l + \delta_i = 4\varepsilon_2\lambda \left(2\sum_{l=1}^{i-1} r_l + r_i \right) \times f_{/\text{number}}. \tag{C9}$$

After some arrangements, the following representation can be obtained:

$$\Phi_i = 8\left(\varepsilon_2\lambda \times f_{/\text{number}}\right)^2 \times \left(2i^2 - 2i + 1\right). \tag{C10}$$

ACKNOWLEDGMENTS

The authors thank M.-L. Li for the assistance in producing some of the figures. They also thank the reviewers for helpful comments.

REFERENCES

[1] K. E. Thomenius, "Evolution of ultrasound beamformers," in *Proc. IEEE Ultrason. Symp.*, pp. 1615–1622, 1996.
[2] S. H. Maslak and H. G. Larsen, "Dynamically focused linear phased array acoustic imaging system," U.S. Patent 4 699 009, 1985.
[3] D. Lipschutz, "Delay interpolation for digital phased array ultrasound beamformers," U.S. Patent 5 345 426, 1994.
[4] W. E. Engeler and C. M. W. Daft, "Ultrasonic imaging having wide-bandwidth dynamic focusing," U.S. Patent 5 488 588, 1996.
[5] M. O'Donnell, W. E. Engeler, J. J. Bloomer, and J. T. Pedicone, "Method and apparatus for digital phased array imaging," U.S. Patent 4 983 970, 1991.
[6] K. Jeon, M. H. Bae, S. B. Park, and S. D. Kim, "An efficient real time focusing delay calculation in ultrasonic imaging system," *Ultrason. Imag.*, vol. 16, no. 4, pp. 231–248, 1994.
[7] S. R. Freeman, M. K. Quick, M. A. Morin, R. C. Anderson, C. S. Desilets, T. E. Linnenbrink, and M. O'Donnell, "Delta-sigma oversampled ultrasound beamformer with dynamic delays," *IEEE Trans. Ultrason., Ferroelect., Freq. Contr.*, vol. 46, no. 2, pp. 320–332, 1999.
[8] A. Gee, C. R. Cole, and J. N. Wright, "Method and apparatus for focus control of transmit and receive beamformer systems," U.S. Patent 5 581 517, 1996.
[9] W. E. Engeler, M. O'Donnell, J. T. Pedicone, and J. J. Bloomer, "Dynamic phase focus for coherent imaging beam formation," U.S. Patent 5 111 695, 1992.
[10] M. H. Bae, "Focusing delay calculation method for real-time digital focusing and apparatus adopting the same," U.S. Patent 5 836 881, 1998.
[11] R. A. Beaudin and M. P. Anthony, "Delay generator for phased array ultrasound beamformer," U.S. Patent 5 522 391, 1996.
[12] D. H. Turnbull and F. S. Foster, "Beam steering with pulsed two-dimensional transducer arrays," *IEEE Trans. Ultrason., Ferroelect., Freq. Contr.*, vol. 38, no. 4, pp. 320-333, 1991.
[13] C. M. W. Daft, L. S. Smith, and M. O'Donnell, "Beam profiles and images from two-dimensional arrays," in *Proc. IEEE Ultrason. Symp.*, pp. 775–779, 1990.
[14] S. W. Smith, G. E. Trahey, and O. T. von Ramm, "Two-dimensional arrays for medical ultrasound," *Ultrason. Imag.*, vol. 14, no. 4, pp. 213–233, 1992.
[15] P.-C. Li and M. O'Donnell, "Phase aberration correction on two-dimensional conformal arrays," *IEEE Trans. Ultrason., Ferroelect., Freq. Contr.*, vol. 42, no. 1, pp. 73–82, 1995.
[16] E. D. Light, R. E. Davidsen, J. O. Fiering, T. A. Hruschka, and S. W. Smith, "Progress in two dimensional arrays for real time volumetric imaging," *Ultrason. Imag.*, vol. 20, no. 1, pp. 1–16, 1998.
[17] P. K. Weber, R. M. Schmitt, B. D. Tylkowski, and J. Steck, "Optimization of random sparse 2-d transducer arrays for 3-d electronic beam steering and focusing," in *Proc. IEEE Ultrason. Symp.*, pp. 1503–1506, 1994.
[18] S. S. Brunke and G. R. Lockwood, "Broad-bandwidth radiation patterns of sparse two-dimensional vernier arrays," *IEEE Trans. Ultrason., Ferroelect., Freq. Contr.*, vol. 44, no. 5, pp. 1101–1109, 1997.
[19] B. J. Savord, "Beamforming methods and apparatus for three-dimensional ultrasound imaging using two-dimensional transducer array," U.S. Patent 6 013 032, 2000.
[20] D. L. Liu and R. C. Waag, "Propagation and backpropagation for ultrasonic wavefront design," *IEEE Trans. Ultrason., Ferroelect., Freq. Contr.*, vol. 44, no. 1, pp. 1–12, 1997.

Pai-Chi Li (S'91–M'93–S'93–M'95–SM'01) received the B.S. degree in electrical engineering from National Taiwan University, Taipei, Taiwan, R.O.C. in 1987 and the M.S. and Ph.D. degrees from the University of Michigan, Ann Arbor in 1990 and 1994, respectively, both in electrical engineering: systems.

He was a research assistant with the Department of Electrical Engineering and Computer Science from 1990 to 1994. He joined Acuson Corporation (Mountain View, CA) as a member of the Technical Staff in June 1994. His work in Acuson was primarily in the areas of medical ultrasonic imaging system design for both cardiology and general imaging applications. In August 1997, he went back to the Department of Electrical Engineering at National Taiwan University as Assistant Professor. He then became Associate Professor in August 1998. His current research interests include biomedical ultrasonic imaging and signal processing.

Dr. Li is a member of IEEE, and he was the recipient of the Distinguished Achievement Award in Electrical Engineering: Systems for his outstanding academic achievement at the University of Michigan.

Jing-Jung Huang was born in 1976 in Taiwan, R.O.C. He received the B.S. and M.S. degrees in electrical engineering from National Taiwan University in 1999 and 2001, respectively. His research interest is ultrasonic imaging system design.